Mauna Kea, Hawai'i as an analogue site for future planetary resource exploration: Results from the 2010 ILSO-ISRU field-testing campaign

I.L. ten Kate[1,2], R. Armstrong[3], B. Bernhardt[4], M. Blumers[5], D. Boucher[6], E. Caillibot[7], J. Captain[8], G. Deleuterio[9], J.D. Farmer[10], D.P. Glavin[1], J.C. Hamilton[11], G. Klingelhöfer[5], R.V. Morris[12], J.I. Nuñez[10], J.W. Quinn[8], G.B. Sanders[12], R.G. Sellar[13], L. Sigurdson[6], R. Taylor[14], K. Zacny[15].

[1] NASA Goddard Space Flight Center, Greenbelt, MD 20771

[2] Goddard Earth Science and Technology Center, University of Maryland Baltimore County, Baltimore, MD 21228

[3] Neptec Design Group, Ottawa, ON, Canada, K2K 1Y5

[4] von Hoerner & Sulger GmbH, Schwetzingen, Germany

[5] Institute of Inorganic Chemistry and Analytical Chemistry, Johannes Gutenberg University D 55099 Mainz, Germany

[6] NorCAT, Northern Centre for Advanced Technology, Sudbury, ON, Canada P3A 4R7

[7] Xiphos Technologies, Montreal, QC, Canada H2W 1Y5

[8] NASA Kennedy Space Center, FL 32899

[9] University of Toronto Institute for Aerospace Studies, Toronto, ON, Canada M3H 5T6

[10] School of Earth and Space Exploration, Arizona State University, Tempeh, AZ 85287

[11] Universitt of Hawai'i at Hilo, Hilo, HI 96720

[12] NASA Johnson Space Center, Houston, TX 77058

[13] Jet Propulsion Laboratory, Pasadena, CA 91109

[14] Neptec USA, Houston, TX, 77058

[15] Honeybee Robotics, New York, NY 10001

Abstract

Within the framework of the International Lunar Surface Operation - In-Situ Resource Utilization Analogue Test held on January 27 – February 11, 2010 on the Mauna Kea

volcano in Hawai'i, a number of scientific instrument teams collaborated to characterize the field site and test instrument capabilities outside laboratory environments. In this paper, we provide a geological setting for this new field-test site, a description of the instruments that were tested during the 2010 ILSO-ISRU field campaign, and a short discussion for each instrument about the validity and use of the results obtained during the test. These results will form a catalogue that may serve as reference for future test campaigns.

1. Introduction

Terrestrial analogue environments are places on Earth with geological and environmental characteristics that resemble those that exist on an extraterrestrial body (Léveillé, 2009). The purpose of using these terrestrial analogue sites for planetary missions can be divided into four basic categories: (i) to *learn* about planetary processes on Earth and elsewhere; (ii) to *test* methodologies, protocols, strategies, and technologies; (iii) to *train* highly-qualified personnel, as well as science and operation teams; and (iv) to *engage* the public, space agencies, media, and educators (Lee, 2007 [35], Léveillé, 2009).

The majority of these environments are studied as Mars analogues, such as the hyperarid regions of the Atacama Desert in Chile (Navarró-González et al., 2003), the Antarctic Dry Valleys (Wentworth et al., 2005) and permafrost (Dickson & Rosen, 2003), the Rio Tinto hydrothermal springs in Spain (Amils et al. 2007), and the Egyptian desert (Herry & Paillou, 2006) (for an overview see Léveillé, 2009). An example of a lunar analogue site is the Vredefort dome in South Africa (Gibson et al. 2002). Other sites are selected based on the ability to test a complete mission concept or planning, such as the Lava Mountains, California (Hinze et al., 1967) and the volcanic fields around Flagstaff, Arizona for Apollo astronaut training[1]. Long-term field testing campaigns with more permanent infrastructures are established

[1] http://astrogeology.usgs.gov/About/AstroHistory/astronauts.html (April 1, 2010)

to provide a base for multidisciplinary field research as well development of new technologies for planetary missions, such as the Haughton-Mars Project Research Station at Devon Island, Canada (Lee & Osinski, 2005, PSS), the Arctic Mars Analogue Svalbard Expedition (AMASE) at Svalbard, Norway (Steele et al., 2007, LPSC), the Pavilion Lake Research Project (Lim et al., 2010), and the Pacific International Space Center for Exploration Systems (PISCES) at Hawai'i (Schowengerdt et al., 2007; Duke et al., 2007 - LPSC).

In this paper, we describe a new field test site for lunar missions, at the Mauna Kea volcano in Hawai'i, and present the results of several instruments that were tested, as reference for future analogue testing. The 2010 International Lunar Surface Operation - In-Situ Resource Utilization Analogue Test (ILSO-ISRU, Sanders and Larson, 2010) on the Mauna Kea volcano in Hawai'i was coordinated by the Northern Centre for Advanced Technology (NORCAT) in collaboration with the Canadian Space Agency (CSA), the German Aerospace Center (DLR), and the National Aeronautics and Space Administration (NASA), through the PISCES program.

The primary reasons for selecting this site as a lunar analogue were the following:

1. *Local material.* The fine-grained, volcanic nature of the material is a suitable lunar analogue, and can be used to simulate excavation, site preparation, and oxygen extraction techniques, with results that can be straightforwardly compared to laboratory tests.
2. *Terrain.* The location provides a large number of slopes, rock avalanches, etc. to perform mobility tests in a very confined area. Long range traversing is not possible, but all of the testing was aimed at either site preparation or resource prospecting and for the early tests, the terrain variation was more important than distance.
3. *Logistics.* The presence of a cafeteria, bedrooms, and mechanical shops within a few kilometers of the test site, and access to the Hilo airport and infrastructure

within only two hours driving distance helps to mitigate risk associated with field logistics and operations.

4. Location. Hawai'i is a reasonable 'central location' for multiple space agencies including NASA, CSA, JAXA (Japanese Space Agency), KARI (Korean Space Agency), and other Pacific nation space agencies, and facilitates wide international participation in field campaigns.

The ILSO-ISRU analogue field campaign primarily focused on hardware testing of technologies and systems related to resource identification, extraction, storage and utilization, with a small but growing role designated for *in situ* science measurements. The primary goals of the campaign were:

1. Oxygen (O_2) production from regolith.

2. ISRU product storage, distribution, and utilization

3. Integrate lunar ISRU and science instruments

4. Site preparation

5. Field geology training

6. Field characterization by science instruments.

In this paper, we provide a geological overview for this new field-test site, a description of the instruments that were tested during the 2010 campaign, and present the results of the tests, with a short discussion per instrument about the validity and use of the data. This database will form a catalogue that can serve as reference for future ISRU field test campaigns on Mauna Kea or other terrestrial analogue sites.

2. Geological setting of Hawai'i, Mauna Kea, and the Pu'u Hiwahine test site.

Hawai'ian volcanism is sourced by a mantle plume (Wilson, 1963): a deep-seated magmatic source, likely generated at the core-mantle boundary (Burke & Torsvik, 2006) that for the last ~40 Ma has a relatively stationary, and prior to that slowly southward moving, long-lived position in the mantle (Steinberger et al., 2004;

Tarduno et al., 2003). Given the absence of plate tectonics on the Moon and Mars, there are several other possible sources of volcanism. Impact induced volcanism (Ronca 1966) is one source, however, volcanism could also be of similar origin as Hawai'ian volcanism, resulting in products of similar composition.

Mantle plumes produce basaltic volcanoes on the overlying Pacific plate. Northwestward motion of the Pacific plate moves the volcanoes away from their source, leading to an array of extinct volcanoes from the active volcanoes of modern Hawai'i, increasing in age to the NW along the Hawai'ian-Emperor seamount chain (Fig. 1).

Figure 1. The Hawai'ian-Emperor seamount chain (Portnyagin et al., 2008).

The Big Island of Hawai'i contains five separate shield volcanoes that erupted somewhat sequentially, one overlapping the other, reflecting the continuing northwestward motion of the Pacific Plate over the Hawai'ian hotspot (Clague and Dalrymple, 1987). These are (from oldest to youngest, Wolfe et al., 1997):

* Kohala—extinct
* Mauna Kea—dormant
* Hualālai—active but not currently erupting
* Mauna Loa—active
* Kīlauea—active, erupting continuously since 1983

Mauna Kea is a dormant volcano (peak altitude of 4205 m above sea level, or 10200 m above the ocean floor) on the Island of Hawai'i, or the Big Island, and is the southernmost of the eight main islands of the Hawai'ian Island Chain (Fig. 2). Mauna Kea is about 1 million years old and it last erupted about 4,500 years ago, but is likely to erupt again. Hawai'ian volcanoes evolve through a sequence of four eruptive stages – pre-shield, shield, post-shield, and rejuvenated (Clague and Dalrymple, 1987, 1989), which are distinguished by lava composition, eruptive rate and style, and stage of development. Mauna Kea transitioned from shield to postshield stage 200,000 to 250,000 years ago. This postshield stage can be divided

into two substages, the postshield basaltic substage (240,000–70,000 years ago) and the hawaiitic substage (66,000-4,000 years ago) (Frey et al., 1990), and accumulates at a rate of approximately 0.004 km^3/yr (Wolfe et al., 1997). Postshield lavas are composed of more alkalic basalts (silica-undersaturated and relatively rich in sodium) than the shield-stage basalt. Mauna Kea is the only volcano in the Hawai'ian chain where glacial till is found (Porter, 1979a,b,c), and deposits of three glacial episodes from 150,000 to 200,000 years ago have been preserved: the oldest two (at roughly 150,000 and 70,000 years ago) during the postshield basaltic substage and the youngest (from approximately 40,000 to 13,000 years ago) during the postshield hawaiitic substage (Wolfe et al., 1997).

Figure 2. The geological map of the Island of Hawai'i, or the Big Island (Trusdell et al., 2006). DPG COMMENT: Would be good to combine Figures 2 and 3 and show the location of Mauna Kea and the ILSO-ISRU test site on Fig. 2.

The Pu'u Hiwahine site, where the field testing took place, is a cinder cone located below the summit of Mauna Kea (19°45'39.29" N, 155°28'14.56" W) at an elevation of ~2783 m (Fig. 3). The site is operated by the Pacific International Space Center for Exploration Systems (PISCES).

Figure 3. Map of the PISCES ILSO-ISRU field location called Pu'u Hiwahine. Both sample sites used in this campaign are marked on this picture. Samples from ISRU-1 were collected using Honeybee Robotics deep drills and then investigated by the Multispectral Microscopic Imager (MMI), Mössbauer, and Volatile Analysis by Pyrolysis of Regolith (VAPoR). ISRU-2 was drilled and investigated by the Regolith and Environmental Science Oxygen and Lunar Volatile Extraction (RESOLVE) instrument.

3. Basic field operations

The instruments used for this study form a representative set of *in situ* instrumentation that could be included on a future lunar or Mars mission to locate, extract, and identify resources in the near-surface regolith. This instrument suite

covers a wide range of measurements and is comprised of a relative navigation vision system (TriDAR), a ground penetrating radar (GPR), a drill system to provide samples, a multispectral microscopic imager (MMI), a miniaturized Mössbauer spectrometer MIMOS II and the advanced version MIMOS IIA with additional X-ray fluorescence capability, and two volatile analyzers (VAPoR and RESOLVE). While the instruments used in the field test were selected from both the Moon Mars Analog Mission Activity (MMAMA) and Field Science Analog Test (FSAT) solicitations from the Science Mission Directorate (SMD) in NASA and from funding from the Canadian Space Agency, some care and thought was taken in the selection process to ensure instruments and their data were complimentary. The TriDAR and GPR initiated field operations by collecting 3D images of the surface and subsurface at a designated area. From the fused TriDAR and GPR data, ideal subsurface drilling and sampling locations in the area designated ISRU-1 (Fig. 3) were selected. At all selected sites, subsurface samples were obtained by drilling down, using coring drills, auger drills and alcohol cleaned handheld scoops and spatulas. Samples from the coring drill were processed by the RESOLVE volatile analysis package. The augers drilled to depths of 4 meters, while samples were collected at 1-meter intervals using the scoops and spatulas. These samples were then distributed among the different science teams, who analyzed them on their respective instruments. Due to time and logistical constraints, the analyses described in this paper were analyzed either at selected analysis/drilling sites or in the "lab-tents".

4. Instruments

4.1 TriDAR

TriDAR (Neptec Design Group) is a combination-imaging sensor that exploits triangulation and LIDAR technologies, to provide detailed images and guidance information. TriDAR was used to collect 3D surface data for a potential landing region as well as sampling regions for the different science instruments. Neptec's 3Di software tool kit is based on the principle that 3D data can be used in real-time applications over relatively modest bandwidth data links and processes data at the

sensor. Processing the data at the sensor eliminates the collection of redundant data.

4.2 Ground Penetrating Radar (GPR)

The GPR survey was conducted autonomously by a team of two multi-agent teaming (MAT) mobility platforms (Fig. 4) working together towards a common goal. In this case, the goal was to efficiently and autonomously conduct a subsurface survey of the landing pad area selected from surface data obtained by the TriDAR. The mobility platforms were each equipped with a commercially available Noggin 1000 and the NogginPlus Data Acquisition Platform. The GPR survey data was filtered using an application developed by the University of Toronto Institute for Aerospace Studies (UTIAS) and subsequently transferred to a Xiphos Technologies' Hybrid Processing Card (HPC). A remote operator then evaluated the data using a set of geotechnical criteria developed by NORCAT. The GPR data and vision system data are fused using 3D visualization software (Voxler) to produce a 3D surface and subsurface model. The drill sites were selected remotely to evaluate the accuracy of the GPR data and provide ground truth for the selected site.

Figure 4. MAT mobility platforms collecting GPR Survey data in the field. This data will be fused with previously acquired TriDAR surface data. The data fusion will produce a 3D surface and subsurface model.

4.3 Drilling Tools

Two subsurface access instruments were used to acquire soil samples, besides the RESOLVE core drill (see 4.7 RESOLVE). These were 1) the Dutch auger[2] also known as the Edelman auger for shallow samples, provided by NORCAT, and 2) a custom screw auger for deep samples (Fig. 5). The Dutch auger is a manually operate drill and collects samples with a length of maximum 15 cm. The screw auger, build by Honeybee Robotics, came in four, 1m long segments. The screw auger with a drill bit

[2] http://www.benmeadows.com/refinfo/techfacts/augers_introduction_298.htm (April 1, 2010)

at the end was manually driven by a 702 Watt Hilti TE 7A Rotary-Percussive, battery powered drill. In order to penetrate deeper, the sections were screwed together. The auger outside diameter (OD) was 2.5 cm, the root diameter was 1.25 cm and the flute depth (and in turn the thickness of the soil layer between the auger flutes) was 0.6 cm.

Figure 5. Drills used for sampling. Left: the Dutch auger, used to acquire shallow (down to 91 cm) samples in 15 cm increments. Right: the screw auger, used to collect subsurface samples by assembling 1-m drill segments to form a 4-m drill string.

4.4 Multispectral Microscopic Imager (MMI)

The MMI (shown in Fig. 6), employs multi-wavelength light-emitting diodes (LEDs), a substrate-removed Indium-Gallium-Arsenide (InGaAs) focal-plane array (FPA), and no moving parts, to provide multispectral, microscale images in 21 wavelength bands extending from visible wavelengths to 1.75 μm in the infrared (Nuñez et al., 2010). The sensor for the MMI is a substrate-removed InGaAs focal-plane array (FPA) sensitive over a spectral range of 0.47 to 1.75 μm. LED illumination wavelengths are activated singly, in succession, as images are acquired by the FPA, providing a dataset comprised of 21 spatially co-registered microimages. Similar to its predecessor, the MI onboard the Mars Exploration Rovers (Herkenhoff et al., 2003), the MMI provides a spatial resolution (63 μm), field of view (FOV, 40 x 32 mm), and depth of field (5 mm) comparable to that provided by a geologist's hand lens. Because the MMI's InGaAs FPA detector technology does not require cooling, it extends the spectral range to 1.75 μm in the infrared with no increase in mass, as compared to the silicon FPAs used in the current state-of-the-art, *in situ* microimagers.

Figure 6. Field configuration of the MMI.

4.5 Mössbauer spectrometers MIMOS II and MIMOS IIA

The Miniaturised Mössbauer Spectrometer MIMOSII (Fig. 7) is a contact instrument to be placed on rock or soil samples not requiring any sample preparation. MIMOSII instruments are on board the two NASA MER rovers on the surface of planet Mars since January2004 still fully operating after more than 6 years [1–4], and will be on board the Russian Phobos-Grunt mission to be launched end of 2011 [8]. An advanced Mössbauer instrument MIMOS IIA has now been developed for ESA and NASA rover missions to be launched in 2018. Major improvements are the simultaneous acquisition of Mössbauer (MB) and XRF spectra, with highest energy resolution in the XRF mode allowing very precise determination of elemental composition [5-7].

.

The Mössbauer effect (recoil-free nuclear gamma resonance absorption) is the recoil-free emission and absorption of gamma rays by nuclei. When the energies of emitting and absorbing nuclei are identical within the line width of the nuclear transition, the resonant absorption process can take place with a certain probability given by the Lamb-Mössbauer factor f. The f-factor (sometimes called Debye-Waller factor) is large when the Mössbauer nuclei are bound in solid materials and have relatively low ground-state transition energies. Not all elements have suitable nuclear transitions. The isotope ^{57}Fe (2.2% natural abundance) does have a suitable nuclear transition with an energy difference of 14.41 keV between ground and first excited states. An exact energy match between absorbing and emitting ^{57}Fe nuclei would not occur, even if the f-factor is close to maximum (1.0), if the nuclei are in different electronic or magnetic environments or if their speciations (e.g., oxidation, coordination, and mineralogical states) are different. An exact energy match can be made by systematically changing the energy of the emitted or absorbed gamma ray using the Doppler effect in which usually the emitter ^{57}Fe nuclei (the source) are set in motion relative to the absorber (the sample to be analyzed) whose position is fixed.

All MIMOS instruments operate in backscattering geometry. A 57Co source irradiates a sample area in about 10mm distance from the detector surface. MIMOS II is using four square shaped PIN diodes with a sensitive area of 1cm² each. The advanced version MIMOS IIA is equipped with a ring of Silicon Drift Detectors developed by PNSensor GmbH and produced at the MPI semiconductor laboratory. The main goal of the new detector system design was to combine high energy resolution at high counting rates and large detector area while making maximum use of the area close to the collimator of the ^{57}Co Mössbauer source.

Figure 7: The Mössbauer Spectrometer MIMOS II setup in the experiment-box (left; upper & lower pictures) and the MIMOS IIA mounted on the Canadian rover performing in-situ measurements (right). The MIMOS II sensor head is shown in the lower right.

Mössbauer spectra provide information on the Fe oxidation state (e.g., Fe^0, Fe^{2+}, and Fe^{3+}), the Fe coordination state (e.g., tetrahedral and octahedral coordination), and the relative abundance of Fe among oxidation states, coordination states, and Fe-bearing phases. The element Fe, which is multivalent and abundant, provides essential geochemical and mineralogical information. Ferrous iron (Fe^{2+}) is common in many rock-forming minerals (e.g., olivine, pyroxene, ilmenite, (titano)magnetite, and chromite) and secondary minerals (e.g., serpentine and sulfates).

[1] Klingelhöfer et al., J.Geophys.Res. 108(E12)(2003),doi:10.1029/2003JE002138.
[2] Klingelhöfer, et al., Science 306 (2004) 1740.
[3] Morris,etal., Science 305 (2004) 833.
[4] Klingelhöfer, in: M.Miglierini, D.Petridis (Eds.), Mössbauer Spectroscopy in Materials Science, Kluwer Academic Publishers, the Netherlands, 1999.
[5] Lechner,et al., Nucl. Instr. and Meth. A377 (1996) 346.
[6] Alberti et al., Nucl. Instr. and Meth. A568 (2006) 106.
[7] Blumers et al., Nucl. Instr. and Meth. A 5xx (2010?) xxx
[8] D. S. Rodionov, G. Klingelhöfer, E. N. Evlanov, M. Blumers, B. Bernhardt, J. Gironés, J. Maul, I. Fleischer, O. F. Prilutskii, A. F. Shlyk, V. M. Linkin, and C. d'Uston,

The Miniaturized Mössbauer Spectrometer MIMOS II for the Phobos Grunt Mission, ISSN 0038 0946, Solar System Research Vol. 44, No. 5 (2010) pp. 362–370; and in Russian in: Astronomicheskii Vestnik, 2010, Vol. 44, No. 5, pp. 391–399

4.6 Volatile Analysis by Pyrolysis of Regolith (VAPoR)

VAPoR is a pyrolysis mass spectrometer for evolved gas analysis (EGA) based on the concept of the Sample Analysis at Mars (SAM, Mahaffy, 2008) instrument on the 2011 Mars Science Laboratory (MSL) mission. VAPoR is designed to detect volatile species in the atmosphere as well as gases evolved from volatile-bearing minerals including water, noble gases, and hydrocarbons at high priority targets of astrobiological interest including the polar regions of the Moon and Mars. The VAPoR flight instrument will consist of a miniature time-of-flight mass spectrometer (Getty et al., 2010) and a sample manipulation system containing 6 individual ovens that can be heated to at least 1200 °C (ten Kate et al., 2010). The VAPoR field unit used in this study (Fig. 8) consists of a commercial quadrupole mass spectrometer (Stanford Research Systems RGA300), one pyrolysis oven that heats samples to a maximum of 1000 °C, and a turbopump (Pfeiffer Vacuum TSU071E, TC600). For the field tests, samples were heated in the oven from ambient temperature to 800°C at a rate of 20 °C/min using a high voltage power supply (Kikusui PAN70-5A). Gases released from powdered samples (up to 10 mg) were then monitored by the RGA300 mass spectrometer by scanning from 2 to 150 Da in unit mass (1 Da) steps. The evolved gas data obtained by VAPoR were used to determine the bulk chemistry of the soil, estimate water abundances, determine the presence and abundance of aliphatic and aromatic hydrocarbons, and in some cases, make mineral identifications.

Figure 8. The VAPoR field unit.

4.7 Regolith & Environment Science and Oxygen & Lunar Volatile Extraction (RESOLVE)

RESOLVE is a drilling and miniature chemistry plant packaged onto a medium-sized rover that analyzes collected soil for volatile components ~~prior to heating~~by heating the soil and reducing it at high temperatures in the presence of hydrogen to produce water (Fig. 9). The RESOLVE Prototype consists of a 1 meter core drill and crusher known as the EBRC (Excavation and Bulk Regolith Characterization~~, i.e. a Drill and a Crusher~~), a reusable Reactor with internal auger to heat 80 to 100 g samples, the Regolith Volatile Characterization (RVC) subsystem, the Lunar Water Resource Demonstration (LWRD) subsystem, the Regolith Oxygen Extraction (ROE) subsystem, and Ground Support Equipment (GSE). The RESOLVE Prototype processing module can be mounted onto any mobility platform that would accept its current mass and volume configuration. RESOLVE's capabilities include drilling one meter into soil, taking core samples, crushing them into 1 mm particles, delivering them to the Reactor, heating one quarter-meter core sample at a time and driving off volatiles, analyzing the volatiles, using a gas chromatographic column (GC) capturing the water and hydrogen evolved, and extracting oxygen by hydrogen reduction. RESOLVE will collect its own sample cores. The requirements of this instrument package include ability to clearly distinguish between hydrogen and water as well as quantify low levels of those species and other potential lunar polar volatiles such as carbon monoxide, ammonia, methane, and hydrogen cyanide. The RESOLVE Regolith Volatile Characterization (RVC) system was designed to evolve and analyze volatile species from regolith samples.

Figure 9. RESOLVE

5. Sample selection and collection.

The sampling site was characterized using a combination of TriDAR and GPR. Prior to scanning the area, spheres were placed within the TriDAR's expected field of view as seen in Fig. 10.

Figure 10. Field preparation for TriDAR surface data acquisition. The spheres were used to maintain a common coordinate system among teams working on site selection and site verification.

GPS coordinates of each sphere (Fig. 10) were obtained using a Trimble Differential GPS unit. GPS localization is a method of converting three-dimensional scan data captured by the TriDAR into a local frame of reference that is independent of the position of the TriDAR. The result of GPS localization is a three-dimensional transformation matrix that converts TriDAR scan data into a local East-North-Up Cartesian coordinate system. This established a local coordinate system under which a series of lunar ISRU operations could be conducted, including pad site selection, autonomous GPR surveying of the site, and data fusion of the acquired surface and subsurface data. The PadSiteSelect software application (Neptec) combines this information into a graphical representation of a TriDAR scan, based on which the site was selected as suitable for verification by GPR. Height data in PadSiteSelect give an indication of the topography of the area, slope information is provided and the standard deviation indicates the roughness of the analyzed area. This site selection activity is meant to mirror a lunar ISRU mission where robotic precursors are deployed and must survey the surroundings to allow ground operators to select a suitable location to begin construction of a landing site for future lunar modules. Data collected by the TriDAR was downloaded and processed by a remote operator at the Canadian Space Agency's (CSA) Exploration and Development Operations Centre (ExDOC), who then uses the processed data in the selection of an appropriate site for verification. The data obtained from the GPR generated a subsurface map used to identify any rocks or other obstacles that may impede landing pad construction. This map was modeled using Voxler software and is depicted in Fig. 11.

Figure 11. Modeled GPR data.

Fusion of the surface data acquired by the TriDAR data and the subsurface GPR data autonomously collected by the MAT mobility platforms produced a 3D model of the potential landing pad construction site. This resulting model is shown in Fig. 12.

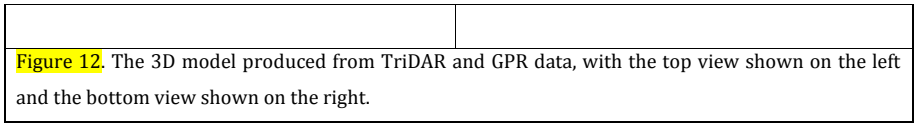

Figure 12. The 3D model produced from TriDAR and GPR data, with the top view shown on the left and the bottom view shown on the right.

Based on the map created by the GPR-TriDAR data, several sample sites were selected. This paper will describe the results obtained from drill site 1, hole 1, also known as ISRU-1, as shown on Fig. 13. The location and altitude of ISRU-1 are given in Table 1 together with the drills used for sampling and their respective sampling depths.

Figure 13. Map of the field-test site and infrastructure, and the location of sample site ISRU-1 (the arrow is added as a guide to the eye).

Table 1. ISRU-1 sample site.

Site	Location	Altitude (m)	Sampling depth for Dutch Auger	Sampling depth for Screw Auger
ISRU-1	N 19° 45' 39.4" W 155° 28' 07.0"	2769.7	Surface to 90 cm	Discrete samples at 1, 2, 3, and 4 m.

The surface at ISRU-1 was covered with dry tephra (the fragmented material produced by a volcanic eruption) layer and had little or no cohesion. The two types of augers used, the Dutch and the screw auger, are normally used when sampling cohesive soils (soils where particles stick to each other such as in wet soils, clay-rich soils, etc), and don't work well in dry, sandy and cohesion-less soils. However, a few inches below the surface the tephra was moist and in turn cohesive and thus relatively easy to sample with the two auger tools. Note that during testing of Apollo drills, in order to increase soil's cohesion, some water was added to the soil mixture, to obtain the required cohesion. Cohesion of lunar soil is a result of the soil particles'

highly angular shape, the presence of agglutinates, and the well-graded (poorly sorted) particles size distribution (Carrier et al., 1991). The auger geometry and soil cohesion was sufficient to retain tephra between the flutes.

The Dutch auger was manually deployed to a depth of 90 cm in 15 cm increments (Fig. 14). Each 15 cm sample weighed >1 kg and was immediately bagged and sealed to avoid contamination and loss of moisture. The subsamples for scientific analysis were taken either just prior to the bagging process or after the samples were bagged.

Figure 14. Sampling with the Dutch auger (would be good to show a picture of a bagged sample).

The sampling procedure for the screw auger included drilling to 1 m depth, pulling the auger out of the hole, taking the samples, cleaning off remainder soil from the auger flutes, attaching additional 1 m segment and drilling to a 2 m depth. This procedure was repeated until 4 m depth was reached. The samples were brushed and/or scraped using a brush or a laboratory spatula directly from the lower part of the auger and into sampling bags (Fig. 15). The soil sampled just above the bit was marked as 1 m, 2 m, 3 m, and 4 m depth sample, depending on the drilling depth.

Figure 15. Sampling with the screw auger. Left: Tephra was captured (DPG COMMENT: Is there a picture showing collection of the drill samples using sterile gloves?) within the auger flutes. Right: Subsample was brushed directly from the flutes closest to the drill bit and into a sampling bag.

The samples collected from ISRU-1 were then analyzed by the MMI, the Mössbauer, and VAPoR.

6. Results – a field-test site database

6.1 Drilling Tools

Drilling to a depth of 4 m was a relatively easy task. In fact, the flutes on the drill auger acted like a screw, and the auger was screwing itself in very fast without need of applying additional vertical force, called Weigh on Bit (WOB). Most of the time, the drill was used in a pure rotary mode (as opposed to rotary-percussive). However, in a few instances where drilling was getting tough (probably when a drill bit encountered occasional rock) a percussive mode was engaged (the drill was used as a rotary-percussive drill) and the penetration rate increased again. With greater depth, we found that the drilling torque would increase – that is the driller had to hold the drill more firm to prevent his hand being twisted. At certain depth, two hands had to be used to prevent the drill from counter rotating. In our previous drilling work in lunar soil simulants, we found that the drilling power required to move cuttings up the flutes is much greater than drilling power required to break-up the formation. This was true not only for compacted lunar soil simulant, but also for ice-saturated and frozen lunar soil simulant, having strength in excess 40 MPa, which is strength of sandstone and limestone (Zacny et al., 2007; Zacny and Cooper, 2007).

The toughest problem, however, was pulling the drill out of the hole. We observed that while the drill was screwing itself in very fast, the auger flutes were getting packed up with cuttings. The end result was the auger got choked up and jammed in a hole (i.e. more cuttings were being generated than what the auger could convey to the surface). We tried reverse and forward rotation while pulling on the drill. This was the only effective method, though very slow. It took two people working at their maximum strength to pull the drill out of the hole in over 20 minutes. We found that the solution to auger chocking was to limit penetration rate by pulling up on the drill, which was certainly counter intuitive. In a conventional drilling process, a driller has to push on the drill and not pull on it. Reducing penetration rate allowed time for cuttings to freely move up the auger flutes. To prevent any future auger jamming occurrences, every so often we would monitor the auger performance. This included pulling the drill up by an inch, while continuing rotation. This was done to determine whether the drill could in fact be still pulled out. If we found that it was

getting tough to pull the drill out, we would increase rotational speed while keeping the drill in place. This allowed excess regolith move up the flutes.

The above findings were exactly what Apollo 15, 16, and 17 astronauts encountered during drilling on the Moon. Apollo 15-17, used the so called Apollo Lunar Surface Drill (ALSD), which was a 460 Watt rotary-percussive, and manually operated drill. The ALSD was used to acquire regolith cores from ~ 3.2 m depth and to drive two hollow casings 2.4 m into the regolith for the two heat flow probes (Apollo 17, 1973; Zacny et al., 2008; Bar-Cohen and Zacny, 2009). The most difficulties were encountered during the first drill deployment on Apollo 15. The two hollow stems for the heat flow probes never reached the required 2.4 m depth; they got stuck below 1 m depth because of poor stem design and resultant insufficient clearing of regolith (the connectors between the two consecutive stems lacked flutes and hence, regolith could not be conveyed to the surface). Although Apollo 15 astronauts, David Scott and James Irwin, did not encounter many problems drilling a core auger to a depth of ~3m, yet they struggled trying to pull it out of the hole. Scott and Irwin had to work at the limit of their combined strength to lift the auger out of the hole, and in the process Scott sprained his shoulder (Apollo 15, 1972). Upon Earth return, the data was analyzed and the drill was subsequently redesigned and new drilling protocols were put in place. In particular, the hollow stems for the heat flow probe were integrated with flutes all the way along their length, astronauts were given a jack to help pulling the drill core out of the hole, and astronauts were asked to deliberately held up on the drill head to slow the penetration rate and hence to allow regolith to move up the auger flutes (Apollo 16, 1973). On Apollo 16 the first section of core was drilled at a rate of approximately 150 cm/min, whereas subsequent drilling was at a rate of approximately 60 to 75 cm/min. Apollo 15 and 17 had similarly high penetration rates.

It is interesting that the drilling rates and the problems encountered on the Moon were very similar to the drilling rates and problems encountered during drilling in Mauna Kea tephra. Therefore, at the end of the field campaign, we concluded that this particular site is an excellent lunar analogue for drilling purposes.

6.2 Multispectral Microscopic Imager, MMI

The Multispectral Microscopic Imager (MMI) characterized the microtexture and mineralogy of materials present. To document depth-related changes in microtexture and mineralogy, we obtained MMI data sets for each one-meter interval, to a total depth of four meters. Applying remote sensing techniques developed for analysis of multispectral imagery, multispectral images were processed and analyzed using the remote sensing and image analysis software package ENVI (a commercial software package sold by ITT Visual Information Solutions). Natural and false color images were prepared while spectral end members (i.e. representing the purest spectra present in the spectral image dataset) were identified and used to produce maps showing the distribution of spectral signatures in the sample. Reflectance spectra (reflectance vs. wavelength) were extracted for the spectral end members and compared to the online USGS spectral library (Clark et al., 2007) to identify best–fit minerals for each spectral end member. Colors of the pixels in the spectral end member maps indicate which spectral end member is the closest match for each pixel. The results presented here compare the surface regolith at ISRU-1 with a subsurface core sample obtained from a depth of two meters.

6.2.1 ISRU-1 surface regolith sample

Figs. 16a and 16b show a natural color image and a spectral end member map of the ISRU-1 surface materials obtained with the MMI. At this site surface sediments consisted of a poorly-sorted volcaniclastic sand. Most grains comprising the coarser size fraction of the regolith (coarse sand to small pebbles) were subrounded and exhibited light-toned to rust-colored alteration rinds. These coatings had spectral features consistent with halide salts that appear to have precipitated on grain surfaces by the evaporation of pore water within the upper capillary fringe zone of the soil. In contrast, the fine sand fraction is a mixture of: 1) dark (unaltered), glassy basalt grains, 2) lighter-toned grains showing rust-colored alteration coatings, or altered grain interiors, and 3) a poorly characterized reddish matrix material of silt to clay-sized particles. Darker grains are finely porphyritic and contain microlites of

light-toned plagioclase feldspars in a black aphanitic to glassy matrix. The presence of magnetite and illmenite is also indicated by the presence of magnetitc grains, particularly in the surface regolith where they appear to have been concentrated by wind erosion.

Figure 16. ISRU-1 surface sample. The natural color image (A) and the spectral end member map (B) obtained with the MMI.

A spectral end member analysis of the surface regolith sample suggests that grain coatings are enriched in Fe-oxides and possibly poorly-ordered clays [see Fig. 17]. Absorption features at MMI bands 1.22, 1.43 µm, and 1.52 µm are overtones of structural OH vibration as well as combination tones of H_2O consistent with the presence of both structurally bound OH/H_2O (~1.43 µm) such as in hydrated minerals like clays or Fe-oxyhydroxides, and pore water (~1.22 µm and 1.52 µm). The depth of these absorptions increases with core depth (compare results for two meter core).

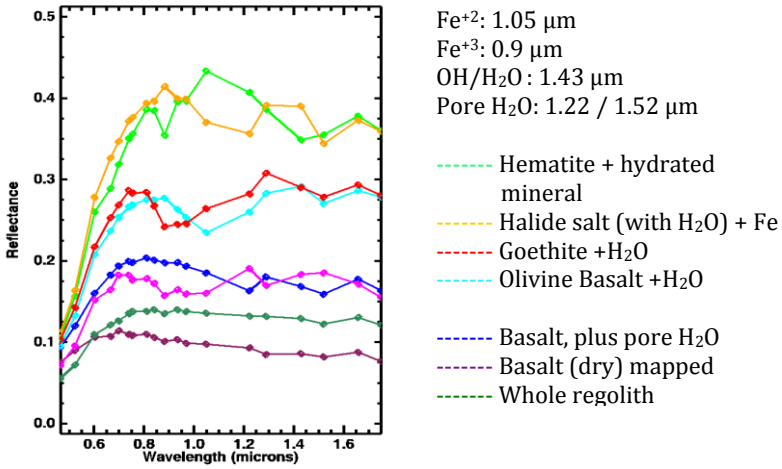

Figure 17. Plot of reflectance versus wavelength for spectral end-members of the surface sample shown in Fig 16b.

6.2.2 ISRU-1 two-meter depth (-2 m) sample

In contrast to the surface sample, the MMI image of the -2 m core sample revealed that the regolith at this depth consisted of fine-grained, well-sorted, volcaniclastic sand (Fig 18). The low reflectance of the sample (as well as high grain cohesion coming out of the corer), suggests an elevated pore-water-content, compared to the surface sample.

Figure 18. ISRU-1 two-meter depth sample. The natural color image (A) and the spectral end member map (B) obtained with the MMI.

The sample has a significant amount of bound water as observed by the absorption feature at 1.43 μm throughout the entire image. The bound water is consistent with the presence of abundant hydrated minerals, including iron oxyhydroxides, such as goethite and ferrihydrite, suggested by the spectral absorptions around 0.90 μm (Fig. 19). This interpretation is also consistent with dark reddish brown phases present in the fine-grained matrix component of the regolith. The fine matrix of the -2 m core at this depth exhibited physical properties (stickiness due to grain-cohesion) consistent with the presence of clays. However, the absence of clay diffraction features in high resolution XRD analysis of the -2 m material in the lab, suggests that this fine component is likely dominated by amorphous weathering products, such as ferrihydrite. Finally, the case for abundant Fe-oxide weathering products in the regolith is further strengthened by the presence of spectral absorptions around 0.90 μm, attributed to Fe^{+3}. The 1.05 μm absorption, interpreted to be due to reduced Fe^{+2} phases, is attributed to the presence of iron-bearing silicates, pyroxene and olivine.

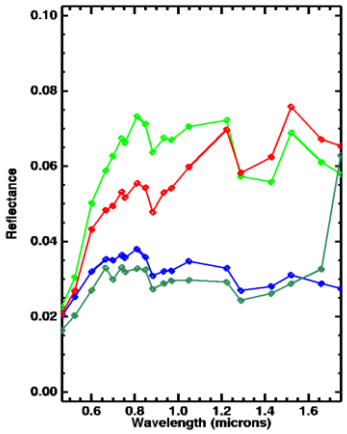

Fe^{+2}: 1.05 µm
Fe^{+3}: 0.90 µm
OH/H_2O: 1.43 µm

---------- Hematite + hydrated mineral
---------- Hematite + hydrated mineral
---------- Basalt matrix + Fe-oxide + hydrated mineral
---------- Whole regolith

Figure 19 Plot of reflectance versus wavelength for spectral end-members of -2 m sample shown in Fig 18b.

The MMI successfully imaged a variety of rock and soil materials under daytime illumination conditions, providing microtextural and compositional information in support of ISRU activities. Spectral analysis of MMI data identified major Fe-bearing silicates and oxides, as well as the presence of hydrated minerals including weathering products such as Fe-oxyhydroxides, placing minerals within a microtextural context to guide sub-sampling of geologic materials for further analysis onboard a rover with other instruments, or in selecting samples for potential return to Earth.

6.3 Mössbauer Results from MIMOS II and MIMOS IIA

During the ISRU field campaign two versions of the miniaturized Mössbauer spectrometer MIMOS II have been used: (i) a copy of the instrument on the Mars-Exploration-Rovers (MIMOS II), and (ii) an advanced version of the MIMOS II called MIMOS IIA, which is equipped with a new detector system allowing in addition to Mössbauer spectroscopy also high-resolution X-ray fluorescence measurements for chemical analysis. Both instruments work in backscattering geometry, which does not require any sample preparation per se. The field of view of both instruments is

circular with a diameter of about 15 mm. The excitation Mössbauer radioactive source is ^{57}Co in a Rhodium metal foil. The instruments have an internal radiation shielding minimizing the external radiation intensity.

The performance of the detector system of both instruments, a Si-PIN-detector system in case of the MIMOS II, and a Silicon-Drift-Detector (SDD) system in case of MIMOS IIA, is temperature dependent and improves with decreasing temperatures, in particular the SDD system. Therefore measurements have been performed also during night-time and early morning to maximize especially the energy resolution of the X-Ray mode of MIMOS IIA.

The two instruments have been operated in both a stationary experiment-box and mounted on the robotic arm of the (NORCAT?) Canadian rover (see fig. Xx in chap. 4.5). The analysis of the samples from ISRU experiments and the analysis of other science samples collected at the test site have been performed in the stationary experiment box. Instrument performance tests with respect to XRF resolution and mobility demonstration have been done with MIMOS II and MIMOS IIA mounted on the robotic arm of the Canadian rover (see for example fig. 20). The Calibration of the two instruments has been done against a metallic Fe foil (see fig. 20). All results are given in respect to metallic Fe.

To monitor the changes of the feedstock material during the ISRU experiments to optimize the oxygen yield, in a first step the Fe mineralogical composition of possible feedstock material was determined. Also some prospect for optimal feedstock material for ISRU O_2 production has been performed together with the ORBITEC team. Several ORBITEC samples have been analyzed during the campaign. They showed different results. The first sinter sample from the Solar Concentrator was highly oxidized. The daytime MB analysis of the second sinter ISRU sample from the Solar Concentrator indicated also that it was highly oxidized (mostly Fe3+) like the other sinter sample (thick melt crust). This sample was a thin (~1 mm) melt crust. From these results some oxygen yields could be calculated. Based on measurement of Fe oxidation states (Fe metal and Fe2+) by Mössbauer spectroscopy on the shinny side of the product from carbothermal reduction, the

oxygen yield for ORBITEC sample 201000203-Exp-2 is ~1 g O/(100g Sample). This yield is a lower limit for the total oxygen yield if other metal oxides are reduced to metal. It also assumes that the Mössbauer measurement at the surface of the charge is representative for the entire sample, and that no Fe-metal is removed by volatilization from the melt during heating. The calculated maximum oxygen yield based on the total Fe concentration (Fe2+ and Fe3+) in the feedstock tephra is ~3 g O/(100g Sample).

Figure 20: (left) Analysis of an ORBITEC sample (20100203-Exp-2) using the Mössbauer Spectrometer MIMOS II (setup in the experiment-box); (right) XRF-spectra for three different samples obtained in-situ with MIMOS IIA on the Canadian (NORCAT?) rover during mobility and positioning tests in the field.

During the whole ISRU campaign the two instruments have been operated successfully 24 hours every day, analyzing science samples from both the ISRU campaign and the test side collected manually or with the Canadian rover. Instrument engineering tests have been performed to validate that Nickel metal hydride (NiMH) batteries perform well as power source for the instrument (draws ~2W). With this the rover/MIMOS IIA configuration for stand-off operations with in situ sample measurement (MB and XRF) has been successfully deployed. In total 8 samples have been analyzed in situ during ~10.5 hr of stand-off operations.
Total Engineering data have been acquired for the direct comparison of MIMOS II and IIA performance. This successful field test represented also the first analysis of geologic materials by the current generation of the MIMOS IIA instrument.

6.4 VAPoR

The VAPoR field experiments were conducted as follows: a 10 mg soil or powdered rock sample was inserted into a quartz sample tube holder, which was closed off on both ends with quartz glass wool to prevent the sample from falling out. Both the quartz wool and the quartz tubes were heated at 500 °C for 3 hours in air to remove any organic residue. The quartz tube was then inserted into the sample oven and the

field unit was evacuated to pressures on the order of 10^{-7} mbar. Since the mass spectrometer only operates at pressures below 10^{-4} mbar, samples were often heated to 50 °C to minimize the internal pressure build-up of the instrument due to adsorbed water in the sample. When the desired operational pressure was reached, the oven ramp (rate of 20 °C/min to 800 °C) was initiated and the mass spectrometer was powered on to begin recording mass spectra as a function of oven temperature.

VAPoR analyzed samples collected from the surface, 2 meters depth (-2 m), and 4 meters depth (-4 m) at ISRU-1. For this study, we focused on the following organic and inorganic species, as listed in Table 2.

Table 2. VAPoR species of interest

Organics			Inorganics		
Name	Formula	Plotted mass	Name	Formula	Plotted mass
Methane	CH_4	13	Water	H_2O	19†
Benzene	C_6H_6	78	Carbon dioxide	CO_2	44 (×0.1)
Toluene	C_7H_8	92	Nitrogen/Carbon monoxide	N_2 / CO	28 (×0.1)
Characteristic alkane fragments		39, 43, 57	Sulfur dioxide	SO_2	64
			†$H_2{}^{17}O$		

Figs. 21 and 22 show the evolved gas profiles for the inorganic compounds (Fig. 19) and organic compounds (Fig. 20) in the samples collected at different depths.

Figure 21. Inorganic volatile content of the surface, -2 m, and -4 m samples from the ISRU-1 sampling site. The peak at mass 19 corresponding to water, saturated the RGA detector at 4 m depth. DPG COMMENT: Can you expand the CO, CO_2 y-axes. You should also consider adding SO_2 and say something about evolved gas profiles of these and how they correlate with presence of sulfate, carbonate minerals, etc. (presence of Goethite detected by MMI for example).

Formatted: English (U.S.), Subscript

Formatted: English (U.S.), Subscript

Figure 22. Volatile organic content of the surface, -2 m, and -4 m samples from the ISRU-1 sampling site. The signal at mass 39 and mass 43 corresponding to alkanes saturated at 4 m depth

The VAPoR results, like the MMI results, clearly show increasing water abundances with depth. The 4 m sample contained so much water that the temperature ramp had to be stopped and held at 300 °C for 30 minutes to lower the internal pressure of the instrument by pumping out the excess water since high background pressures saturate and will eventually damage the mass spectrometer. The double peak in the 4 m depth plots is caused by saturation of water and hydrocarbons released from the sample. The 4 m samples were visually very wet; nearly muddy upon collection therefore results from the evolved gas analysis results of this sample were not surprising. The surface has a much lower abundance of water and some organic fragments, which could be due to the harsher surface conditions, such as wind- and surface erosion. The abundance of organics increased substantially with depth, suggesting that organics have leached downward with the water..

The VAPoR instrument operated as anticipated, however, in-depth analysis of the data is inhibited by the high outgassing caused by the water content of some of the samples. This could have been prevented by analyzing a smaller sample (on the order of 1-2 mg instead of 10 mg), but given our schedule in the field, it was decided to run samples collected from other drill sites. For the field tests, a new high temperature alumina coated tungsten wire crucible (RD Mathis) was used in the VAPoR field tests. Prior to deployment, this oven was baked out in the laboratory to 1000 °C to reduce outgassing from the alumina crucible.. Blank analyses (empty oven), between soil samples were analyzed for background volatile corrections, however, even after 12 heating cycles up to 800°C, outgassing products (e.g water, alkane fragments) from the oven itself were still observed. As described by ten Kate et al. (2008) contamination is an important issue in missions looking for organics, and volatile outgassing from high temperature oven materials should be minimized. Therefore it is difficult to draw any final conclusions on especially the exact organic content of the analyzed samples. The higher water and organic content at lower

depths is however not considered to be an artifact of the instrument, but indeed a real observation from the samples.

6.5 RESOLVE

One of the goals of this field test was to demonstrate the detection of low levels of hydrogen and water evolved during heating of a tephra sample. These low levels of hydrogen and water were obtained by drying the collected sample and then doping it with water and metal hydride. *Water doping* of the soil was performed by two methods. The first method was to simply expose the dried and sieved tephra sample to atmospheric conditions. The tephra absorbs a small amount of water from the moisture in the atmosphere, typically coming to a water content of about 1% by weight. Higher water concentrations of water were achieved by doping a small amount of tephra with liquid water and adding the doped sample to the reactor. In this manner up to an additional 0.5 grams of water was added to the reactor. Both doping methods were used in the field in an effort to illustrate the detection ranges of the GC. *Hydrogen doping* was performed by manually adding metal hydride (Hy-stor 207, lanthanum nickel aluminum metal hydride) to the regolith sample. This metal hydride had the desirable range of vapor pressure (0.43 bar at 25 °C to 42.6 bar at 175 °C) and was passivated to ensure safe operations in air. To prevent a flammable mixture of gas in the reactor during heating, the reactor was purged with argon prior to heating. The instrument was calibrated with known amounts of water and hydrogen prior to the field test.

The 82.3 g sample core described in this paper was collected by RESOLVE at site ISRU-2, on top of the ridge (see Fig. 3) and prepared in the field by sieving and drying. The sample was then transferred to the reactor and doped with the water bearing tephra and metal hydride. Subsequently the sample was heated to 150 °C over approximately an hour. Evolved gases were fed into the GC, which was optimized for H_2, He, and water detection. The separation of water, CO_2 and inert species was performed on a Porabond-Q column, with a heart cut to separate the

inert species on a mol-sieve column using a Deans switch. As the sample was heated, both hydrogen and water evolved with increasing temperature as shown in Fig. 20.

Figure 20. Gas evolution in the RESOLVE reactor. Hydrogen, water, and carbon dioxide were measured as target gases; argon gas was used to purge the reactor before heating and does not evolve from the sample at these temperatures.

Prior to the transfer of the sample from the reactor to the surge tank, the gas composition in the reactor was 39.4% hydrogen, 6.9% argon, 9.5% carbon dioxide, and 44% water. These values were converted to masses assuming the ideal gas law using the pressure, volume and temperature of the reactor. The results are shown in Table 3. These results show that the RESOLVE gas analysis system is able to analyze very low weight percents of volatiles in tephra, well below 0.1% by weight.

Table 3. Mass and weight percent of hydrogen, water, and carbon dioxide evolved from the sample collected at ISRU-2.

	Hydrogen	Water	Carbon Dioxide
Mass (g)	0.0037	0.0371	0.0196
Weight %	0.0045	0.0451	0.0238

The RESOLVE prototype has shown end-to-end operation of volatile detection during the 2010 field campaign, showing advancements towards flight operation. The current system highlights a re-useable reactor that facilitates volatile identification and quantification. Successful low level of detection of water and hydrogen during an analogue mission highlight the ability of this system to detect and quantify lunar volatiles. Future work for RESOLVE must include further miniaturization, improvements to dust tolerant seals, addition of a mass spectrometer detector to the GC analysis, and improved thermal characteristics of the system.

DPG COMMENT: We should explain why samples from ISRU-1 were not analyzed by RESOLVE.

7. Summary

In this paper we provide a description and regional geological setting for a new field analogue test site for lunar resource exploration, and discuss results obtained from the 2010 ILSO-ISRU field campaign as a reference for future field-testing at this site. The following instruments were tested: a multispectral microscopic imager, MMI, a Mössbauer spectrometer, an evolved gas analyzer, VAPoR, and an oxygen and volatile extractor called RESOLVE. Preliminary results show that the sediments change from dry, organic-poor, poorly-sorted volcaniclastic sand on the surface, containing basalt, iron oxides and clays, to more water- and organic-rich, fine grained, well-sorted volcaniclastic sand, primarily consisting of iron oxides and depleted of basalt and clays. Furthermore, drilling experiments showed a very close correlation between drilling on the Moon and drilling at the test site. The ILSO-ISRU test site was an ideal location for testing strategies for *in situ* resource exploration at the lunar or martian surface.

Acknowledgements

The authors would like to thank and acknowledge the Canadian Space Agency and NASA for funding the analog field test infrastructure and campaign, NORCAT for providing analog field test site infrastructure, and the Pacific International Space Center for Exploration Systems (PISCES) for obtaining access to the analog field test site and providing logistics and assistance for field test operations. The authors would also like to thank ~~CSA and NORCAT for logistics support and~~ the NASA ROSES Field Science Analogue Testing (FSAT), Astrobiology Science and Technology Instrument Development (ASTID), and Moon and Mars Analogue Mission Activities (MMAMA) programs for instrument funding and field science support. GK, BB and MB acknowledge the support by the German Space Agency DLR under contract 50QX0802..

References

Apollo 15 Mission Report, (1973), http://history.nasa.gov/alsj/a15/a15mr.htm

Apollo 16 Mission Report, (1973), http://history.nasa.gov/alsj/a16/a16mr.html

Apollo 17 Mission Report, (1973), http://www.hq.nasa.gov/alsj/a17/a17mr.html

Bar Cohen, Y., and K. Zacny, (2009), Drilling in Extreme Environments: Penetration and Sampling on Earth and other Planets, Wiley-VCH (September 15, 2009)

Burke K. and Torsvik T.H. (2004) Derivation of Large Igneous Provinces of the past 200 million years from long-term hetergeneities in the deep mantle. *Earth and Planetary Science Letters*, 227, 531-538.

Carrier W.D. III, Olhoeft G.R., and Mendell W. (1991) Physical properties of the lunar surface, in Lunar Sourcebook (G.H. Heiken, D.T. Vaniman, and B.M. French, Eds.), Cambridge University Press, Cambridge, 736 pp.

Clague D. A. and Dalrymple G. B. (1987) The Hawai'ian-Emperor volcanic chain. Part I. Geologic evolution, In *Volcanism in Hawai'i*, edited by Decker R. W., Wright T. L., and Stauffer P.H., U. S. Geological Survey Professional Paper 1350(1), 5-54.

Clague D. A. and Dalrymple G. B. (1989) Tectonics, geochronology, and origin of the Hawai'ian-Emperor Chain. In *The eastern Pacific Ocean and Hawai'i*, edited by Winterer E. L., Hussong D. M. and Decker R. W., Geological Society of America, The Geology of North America 188-217.

Clark, R. N., G. A. Swayze, R. Wise, E. Livo, T. Hoefen, R. Kokaly, and S. J. Sutley, 2007. USGS Digital Spectral Library splib06a: U.S. Geological Survey, Digital Data Series 231.

Frey F. A., Wise W. S., Garcia M. O., West H. B., Kwon S.-T., and Kennedy A. (1990) Evolution of Mauna Kea Volcano, Hawai'i: Petrologic and geochemical constraints on postshield volcanism. *Journal of Geophysical Research*, 95(B2), 1,271-1300.

Herkenhoff, K. E., S. W. Squyres, J. F. Bell, J. N. Maki, H. M. Arneson, P. Bertelsen, D. I. Brown, S. A. Collins, A. Dingizian, S. T. Elliott, W. Goetz, E. C. Hagerott, A. G. Hayes, M. J. Johnson, R. L. Kirk, S. McLennan, R. V. Morris, L. M. Scherr, M. A. Schwochert, L. R. Shiraishi, G. H. Smith, L. A. Soderblom, J. N. Sohl-Dickstein, and M. V. Wadsworth, 2003. Athena Microscopic Imager Investigation. *J. Geophys. Res.* 108(E12), 8065, doi:10.1029/2003JE002076.

Lim D. S. S., Abercromby A.F., Andersen D., Andersen M., Arnold R.R., Bird J.S., Bohm H.R., Brady A.L., Cady S.L., Cardman Z., Chan A.M., Chan O., Chénard C., Cowie B.R., Davila A., Deans M.C., Dearing W., Downs M., Fong T., Forrest A., Gernhardt M.L., Hawes I., Hansen J., Imam Y., Laval B.L., Lees D., Leoni L., Looper C., Marinova M.M., McCombs D., McKay C.P., Mullins G. Nuytten, P. Pendery R., Pike W., Pointing S.B., Pollack J., Raineault N., Reay M., Reid D., Sallstedt T., Schulze-Makuch D., Seibert M., Shepard R., Slater G.F., Sumner D.Y., Suttle C.A., Trembanis A., Turse C., Wilhelm M., Wilkinson N., Williams D., Winget D.M., Winter C. (2010) The Pavilion Lake Research Project – A Deep Dive towards the Moon and Mars. *Geological Survey of America* Special Issue (in review).

Nuñez, J. I., J. D. Farmer, R. G. Sellar, and C. C. Allen (2010). The Multispectral Microscopic Imager: Integrating Microimaging with Spectroscopy for the In-Situ Exploration of the Moon. *41st Lunar and Planetary Science Conference*, The Woodlands, TX, March 1-5, 2010. Abstract #1581.

Porter S. C. (1979a) Quaternary stratigraphy and chronology of Mauna Kea, Hawai'i: a 380,000-yr record of mid-Pacific volcanism and ice-cap glaciation: Summary. *Geological Society of America Bulletin*, pt. 1, 9(7), 609-611.

Porter S. C. (1979b) Quaternary stratigraphy and chronology of Mauna Kea, Hawai'i: A 380,000-yr record of mid-Pacific volcanism and ice-cap glaciation. *Geological Society of America Bulletin*, pt. 2, 90(7), 980-1,093.

Porter S. C. (1979c) Hawai'ian glacial ages. *Quaternary Research*, 12, 161-187.

Sanders, G. B. and Larson, W. E. (2010) Integration of In-Situ Resource Utilization Into Lunar/Mars Exploration Through Field Analogs. *Advances in Space Research*. doi: 10.1016/j.asr.2010.08.020

Stearns H. T. (1945) Glaciation of Mauna Kea, Hawai'i. *Geological Society of America Bulletin* 56(3), 267-274.

Steinberger B., Sutherland R., and O'Connell R. J. (2004) Prediction of Emperor-Hawai'i seamount locations from a revised model of global plate motion and mantle flow. *Nature* 430, 167-173.

Tarduno J. A., Duncan R. A., Scholl D. W., Cottrell R. D., Steinberger B., Thordarson T., Kerr B. C., Neal C. R., Frey F. A., Torii M., and Carvallo C. (2003) The Emperor Seamounts: Southward motion of the Hawai'ian hotspot plume in earth's mantle. *Science* 301, 1064-1069.

Trusdell F. A., Wolfe E. W., and Morris J. (2006) Digital database of the geologic map of the Island of Hawai'i: U.S. Geological Survey Data Series 144 [available on the World Wide Web at http://pubs.usgs.gov/ds/2005/144/].

Formatted: Font: Italic

Wilson J. T. (1963) A possible origin of the Hawai'ian Islands. *Canadian Journal of Physics* 41, 863-870.

Wolfe E .W., Wise S. W., and Dalrymple G. B. (1997) The geology and petrology of Mauna Kea Volcano, Hawai'i -- A study of postshield volcanism. *U.S. Geological Survey Professional Paper* 1557, 129, 4 plates.

Zacny, K., Bar-Cohen, Y., Boucher, D., Brennan, M., Briggs, G., Cooper, G., Davis, K., Dolgin, B., Glaser, D., Glass, B., Gorevan, S., Guerrero, J., Paulsen, G., Stanley, S. and Stoker, C. (2008). "Drilling systems for extraterrestrial subsurface exploration." Astrobiology, 8 (3), 665–706, DOI:10.1089/ ast.2007.0179.

Zacny, K., D. Glaser, P. Bartlett, K. Davis, and S. Gorevan, (1997) Drilling Results in Ice-Bound Simulated Lunar Regolith, Space Technology and Applications International Forum 2007, February 11-15, 2007, Albuquerque, New Mexico.

Zacny K., and G. Cooper, (2007) Methods For Cuttings Removal from Holes Drilled on Mars, Mars Journal, Mars 3, 42-56, 2007, doi:10.1555/mars.2007.00